Dynamic Simulation of Primary Particle-Size Distribution in Vinyl Chloride Polymerization

C. KIPARISSIDES,* D. S. ACHILIAS, and E. CHATZI

Chemical Engineering Department and Chemical Process Engineering Research Institute, Aristotle University of Thessaloniki, P.O. Box 472, Thessaloniki, Greece

SYNOPSIS

In the suspension polymerization of vinyl chloride, colloidally stable primary particles are formed inside the polymerizing monomer droplets. The nucleation, growth, and aggregation of these particles are responsible for the formation of the internal particle morphology and associated properties, such as pore-size distribution, specific surface area, and plasticizer uptake. In the present investigation, a population balance model is derived describing the time evolution of the primary particle-size distribution in the polymerizing monomer droplets. The resulting integrodifferential equation accounts for the coalescence rate of electrically charged colloidal primary particles through the use of the Fuchs modification of the extended Smoluckowski coagulation equation. Simulation studies were carried out to determine both the effects of the model parameters and to afford a direct comparison of model predictions with experimental measurements of the time evolution of the primary particle-size distribution. The dependence of the total number and of the mean diameter of the primary particles on several process variables (i.e., the ionic strength of the medium, total particle charge, temperature, initial initiator concentration, and agitation rate) is quantitatively analyzed. Finally, the predictive capability of the present model is demonstrated by a direct comparison of model predictions with the experimental data of Willmouth et al. and Törnell and Uustalu. © 1994 John Wiley & Sons, Inc.

INTRODUCTION

Poly (vinyl chloride) (PVC) is one of the oldest polymers and the second largest in volume thermoplastic manufactured in the world.[1] The enormous expansion of the PVC industry is due to the high versatility of PVC as a plastic raw material. A review of the qualitative and quantitative aspects of PVC polymerization can be found in reviews by Butters,[2] Burgess,[3] Rance,[4] and Langsam[5] and more recently by Törnell,[6] Xie et al.,[7,8] and Yuan et al.[9]

PVC is effectively insoluble in its own monomer; thus, vinyl chloride monomer (VCM) polymerization is a heterogeneous process that involves several physical transitions during the polymerization. As a result, the final particulate product is made up of primary particles and its aggregates. The nucleation, growth, and aggregation of these particles are responsible for the internal morphology of the particulate PVC and its associated properties such as pore-size distribution and specific surface area. In what follows, a brief review of the physical phenomena taking place during VCM polymerization is presented.

The formation of primary particles has been the subject of numerous investigations over the past 30 years.[10-31] According to Rance[4,15] and Allsopp,[17] the mechanism of nucleation, growth, and aggregation of PVC primary particles includes the following stages:

Stage 1: Primary radicals formed by the thermal fragmentation of initiator rapidly react with monomer molecules to produce PVC macromolecules that are insoluble in the monomer phase. Aggregation of the closely spaced polymer chains results in the formation of unstable polymer microdomains with di-

* To whom correspondence should be addressed.

Journal of Applied Polymer Science, Vol. 54, 1423–1438 (1994)
 CCC 0021-8995/94/101423-16

ameters in the range of 10–20 nm (conversion $\leq 0.01\%$).

Stage 2: Due to the very limited stability of the microdomains, they rapidly aggregate to form the primary particle nuclei, also called domains. The initial size of these domains lies in the range of 80–100 nm (conversion range, 0.01–10%).

Stage 3: The primary particles carry negative electrostatic charges; hence, they form stable colloidal suspensions in the monomer phase. In the early stages of the polymerization (conversion $< 5\%$), primary particles grow in size mainly by capturing unstable microdomains and, to a lesser degree, by polymerization of the absorbed monomer.

Stage 4: At conversions around 10–30%, primary particles start aggregating and form a continuous polymer network throughout the VCM droplet. The primary particles continue to grow until the disappearance of the free monomer phase (e.g., conversion of about 75%). The final size of the primary particles is in the range of 1000–1500 nm. Aggregates formed by coalescence of primary particles are in the size range of 3–10 μm.

Stage 5: Finally, at higher monomer conversions, primary particles fuse together. The conversion at which the primary particles fusion occurs is about the same as the conversion at which the free monomer phase disappears.

Willmouth et al.[19] and Törnell et al.[22,27] investigated experimentally the dependence of the total number and of the mean diameter of the primary particles on the VCM conversion during the early stages of polymerization. The development of structure within the grains of suspension PVC (e.g., conversions 5–85%) was experimentally investigated by Smallwood.[25] Despite the different polymerization conditions employed (i.e., temperature, stirrer speed, etc.), it was found that the primary particles reached the same limiting values of 1.4 μm for the average particle diameter and 2.0×10^{11} primary particles per cm^3. Furthermore, Smallwood[32] showed that the final porosity of the product was strongly related to the conversion at which the primary particles network was first formed.

Despite the fact that the end-use properties of particulate PVC are strongly related to the particle morphology, there is only limited work published in the open literature dealing with the development of quantitative models describing the size evolution of primary particles in terms of the process conditions. This is undoubtedly due to the complexity of physical and chemical phenomena taking place in a polymerizing monomer droplet, as well as the formulation and solution of the resulting population balance equation. Ray et al.[33] presented a model for the prediction of the PVC primary particle-size distribution using a semiempirical form for the calculation of the particle coalescence rate constant. Kiparissides[34] developed a population balance model to describe the time evolution of the primary particle-size distribution as a function of the process variables such as temperature, ionic strength of the medium, and type and amount of steric stabilizer. Later on, Kiparissides et al.[35] derived detailed expressions for the calculation of the coalescence rate constant of two colloidal particles by taking into account both electrostatic and steric stabilization forces.

The aim of the present study was to develop a comprehensive mathematical model for the quantitative prediction of the evolution of primary particle-size distribution during the free-radical polymerization of VCM. The present model has the ability to predict the dynamic behavior of the primary particle population from the start of polymerization up to the formation of particle aggregates. It is based on the model and detailed expressions developed by Kiparissides et al.[34,35] and describes quantitatively the effect of the most important process variables, such as temperature, the initial concentration of initiator, the ionic strength of the medium, and the particle charge density on the formation, growth, and aggregation of primary particles. One of the most important developments in this study is the excellent agreement obtained between the theoretical model predictions and the experimental results of Willmouth et al.[19] and Törnell and Uustalu.[27]

POPULATION BALANCE MODEL

A typical PVC suspension polymerization reactor is shown in Figure 1. The magnified portion of the suspending medium shows a VCM droplet during the initial stages of polymerization. Droplet coalescence is typically controlled by the addition of primary and secondary suspending agents. Inside the monomer droplet, one can identify the polymer microdomains as well as the primary particles. The microdomains initially formed have a diameter of about 20 nm. They rapidly coalescence to form the nuclei of domains having diameters in the range of 100–200 nm.

The population balance equation describing the evolution of the primary particle-size distribution

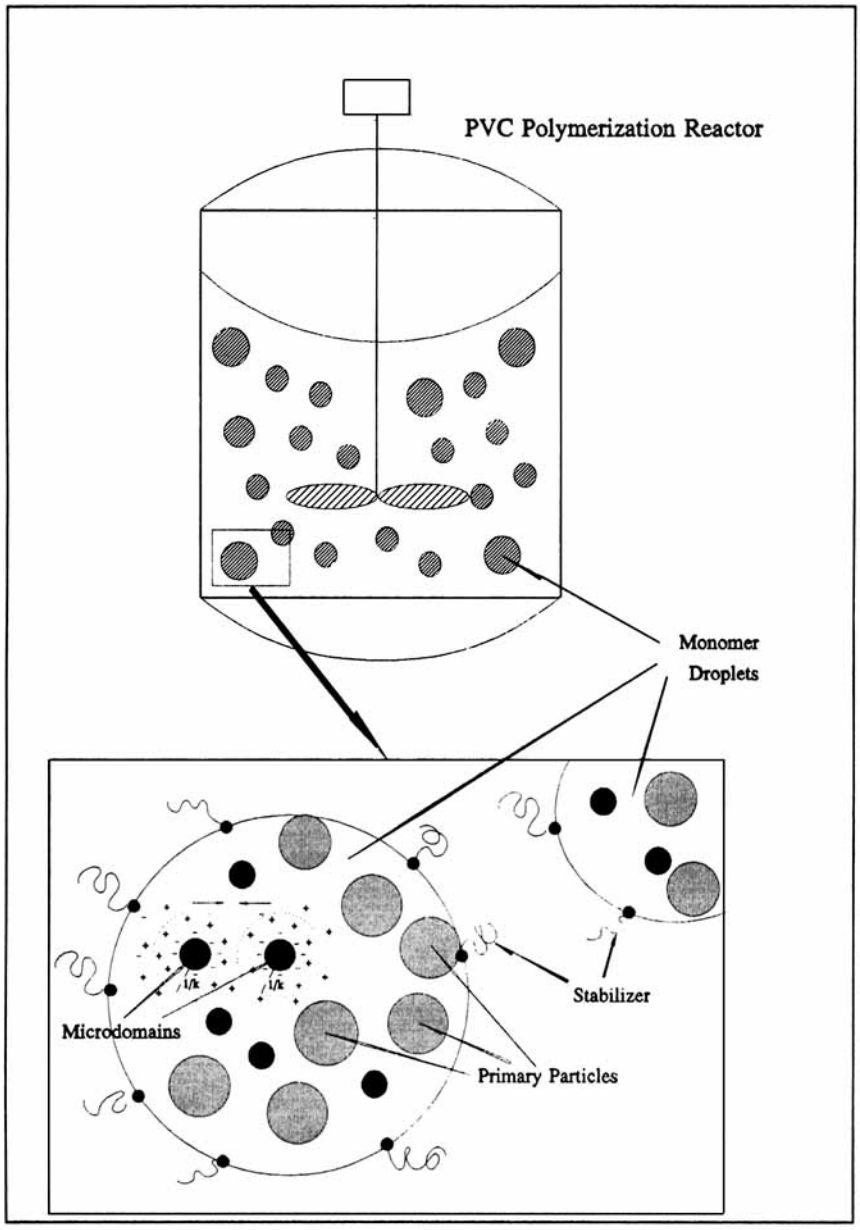

Figure 1 Schematic representation of the electrostatic stabilization of PVC primary particles in a polymerizing monomer droplet.

inside a polymerizing VCM droplet has been derived by Kiparissides[34] and has the following general form:

$$\frac{\partial n_v(V,t)}{\partial t} + \frac{\partial[I_v n_v(V,t)]}{\partial V} = \frac{1}{2}\int_{v_0}^{v-v_0} \beta(V-U,U)n_v(V-U,t)n_v(U,t)\,dU - \int_{v_0}^{\infty} \beta(V,U)n_v(V,t)n_v(U,t)\,dU \quad (1)$$

The initial as well as the boundary conditions required for the integration of eq. (1) are expressed as

$$n_V(V,0) = 0.0; \quad t = 0 \quad (2)$$

$$\frac{\partial n_v(V_0,t)}{\partial t} = -n_v(V_0,t)\int_{v_0}^{\infty} \beta(V_0,U)n_v(U,t)\,dU + r(V_0,t); \quad t > 0; \quad V = V_0 \quad (3)$$

where $n_v(V, t)$ is the number-volume density function. The term $n_v(V, t)dV$ denotes the number of particles of volume V to $V + dV$ at time t per unit volume of the reaction medium. Equation (1) expresses the change of the density function $n_v(V, t)$ with respect to time (first term) and particle volume due to polymerization in the polymer-rich phase (second term). The first term on the right-hand side of eq. (1) accounts for the rate of generation of particles in the size range V to $V + dV$ due to agglomeration of two particles of volumes $V - U$ and U. The factor $\frac{1}{2}$ that multiplies this term accounts for the double counting of particle pairs appearing in the integration. Finally, the last term of eq. (1) represents the rate of disappearance of particles in the size range V to $V + dV$ due to agglomeration of a particle of size V with particles of any other size. The term $r(V_0, t)$ in eq. (3) represents the rate at which basic particles (i.e., microdomains) of volume V_0 are generated due to polymerization and chain precipitation in the monomer-rich phase.

It is often more practical to use the number-diameter density function, $n_D(D, t)$, instead of the number-volume distribution. Accordingly, $n_D(D, t)\,dD$ represents the number of primary particles in the size range D to $D + dD$ at time t per unit volume of the reaction medium (no. particles/(m_r^3)). It can be shown that $n_D(D, t)$ is related to $n_v(V, t)$ according to the following equation:

$$n_D(D, t) = n_v(V, t)\frac{dV}{dD} = n_v(V, t)\frac{\pi D^2}{2} \quad (4)$$

Using eq. (4), the population balance eq. (1) can be expressed in terms of the number-diameter density function as

$$\frac{\partial n_D(D, t)}{\partial t} + \frac{\partial[I_D n_D(D, t)]}{\partial D} = \frac{1}{2}\int_{D_0}^{(D^3 - D_0^3)^{1/3}} \beta(D', \Delta) n_D(D', t) n_D(\Delta, t) \times D^2\Delta^{-2}\,dD' - n_D(D, t) \times \int_{D_0}^{\infty} \beta(D', D) n_D(D', t)\,dD' \quad (5)$$

where

$$\Delta = (D^3 - D'^3)^{1/3}; \quad V = \frac{\pi D^3}{6}; \quad U = \frac{\pi D'^3}{6} \quad (6)$$

The initial as well as the boundary conditions required for the integration of eq. (5) are expressed as

$$n_D(D, 0) = 0.0; \quad t = 0 \quad (7)$$

$$\frac{\partial n_D(D_0, t)}{\partial t} = -n_D(D_0, t)\int_{D_0}^{\infty} \beta(D_0, D') n_D(D', t)\,dD' + r(D_0, t); \quad t > 0; \quad D = D_0 \quad (8)$$

Calculation of the Rate of Formation of Microdomains

The rate of generation of microdomains, $r(V_0, t)$, will depend on the rate of polymerization in the monomer-rich phase R_{pm} and will be given by

$$r(V_0, t) = \frac{R_{pm} M_w}{d_p(1 - \varphi_m)V_0^2} \quad (9)$$

where M_w, d_p, and φ_m denote the monomer molecular weight (62.5 for VCM), the density of PVC $\{10^3 \exp[0.4296 - 3.27410^{-4}\,T(\mathrm{K})]$, g/L$\}$ and the equilibrium monomer volume fraction in the polymer-rich phase, respectively. The latter can be expressed as

$$\varphi_m = \frac{1 - X_c}{1 - X_c(1 - d_m/d_p)} \quad (10)$$

where X_c is the critical conversion at which the separate monomer phase disappears $[0.8 - 1.910^{-3}\,T(°\mathrm{C})]$. d_m and V_0 denote the density of the monomer $[947.1 - 1.746\,T(°\mathrm{C}) - 3.2410^{-3}\,T^2(°\mathrm{C})]$ and the initial volume of the microdomains, respectively.

Calculation of the Primary Particle Growth Rate

The rate of growth of the primary particles due to polymerization of the absorbed monomer in the polymer-rich phase, I_V, can be expressed in terms of the overall rate of polymerization in the polymer-rich phase, R_{pp}, using the following equation:

$$I_V = \frac{R_{pp}}{[M_0]X} V \quad (11)$$

where $[M_0]$ and X are the initial monomer concentration and the fractional conversion, respectively. The growth rate of primary particles in terms of

particle diameter can be obtained from eq. (11) by substituting V by $\pi D^3/6$.

Calculation of the Polymerization Rates

The kinetics of VCM polymerization has been the subject of numerous publications over the last 25 years.[7,8] The mathematical models proposed to describe the evolution of the polymerization rate have been recently reviewed by Sidiropoulou and Kiparissides[36] and Xie et al.[7,8] It is beyond the scope of the present investigation to examine which model describes best the kinetics of the VCM polymerization.

Based on the pertinent phenomena of VCM polymerization described in the Introduction of this paper, it is obvious that phase separation occurs at very low monomer conversions (e.g., $X < 0.001\%$). For kinetic modeling purposes, it is reasonable to assume that polymerization occurs in both the monomer and polymer phases from the very beginning of the polymerization. According to Abdel-Alim and Hamielec,[37] the rates of polymerization in the monomer-rich as well as in the polymer-rich phase (R_{pm}, R_{pp}) are given by

$$R_{pm} = k_p[M][R^*]\frac{X_c - X}{X_c(1 - X)} \tag{12}$$

$$R_{pp} = k_p[M][R^*]PX\frac{1 - X_c}{X_c(1 - X)} \tag{13}$$

where $[R^*]$ is the total radical concentration given by

$$[R^*] = \left(\frac{2fk_d[I]}{k_t}\right)^{1/2} \tag{14}$$

where $[M]$ and $[I]$ denote the monomer and initiator concentration, respectively, and k_p, k_t, and k_d the corresponding propagation, termination, and initiator decomposition rate constants. f is the initiator efficiency. The overall fractional monomer conversion is obtained from the numerical integration of the following differential equation:

$$\frac{dX}{dt} = k_p[R^*](1 - X - AX + PAX)/(1 - BX)^{1/2} \tag{15}$$

where B is the volume contraction coefficient and the parameters A and P are given by[37]

$$B = \frac{d_p - d_m}{d_m} \tag{16}$$

$$A = \frac{1 - X_c}{X_c} \tag{17}$$

$$P = \frac{(2fk_d/k_t)_p^{1/2}}{(2fk_d/k_t)_m^{1/2}} \tag{18}$$

The value of P is greater than unity and varies with temperature[36] [$P = 27 - 0.14\ T(°C)$].

Calculation of the Coalescence Rate Constant

The term $\beta(V, U)$ or $\beta(D, D')$ appearing in the population balance eq. (1) or (5) denotes the coalescence rate constant of two colloidal particles having volumes U and V or diameters D and D'. Since the initial particle growth occurs mainly by particle aggregation and to a smaller extent by polymerization of the absorbed monomer in the polymer-rich phase,[34] knowledge of analytical expressions for the coalescence rate constant is of profound importance to the solution of the population balance model [eq. (5)].

Kiparissides et al.[35] derived detailed expressions for the calculation of the coalescence rate constant for electrically charged colloidal particles. The coalescence rate constant,[35] $\beta(D_i, D_j)$, is given by the Fuchs[38,39] modification of the extended Smoluchowski coagulation equation:

$$\beta(D_i, D_j) = \beta_{ij} = E_f\frac{2}{3}\frac{kT}{\mu}\frac{(R_i + R_j)^2}{R_iR_j}\frac{1}{W_{ij}} \tag{19}$$

where k, T, μ, and W_{ij} denote the Boltzmann's constant (1.38×10^{-23} J/K), the reaction temperature, the viscosity of the monomer phase[19] [$2.1 \times 10^{-4} - 1 \times 10^{-6}\ T(°C)$, Nsm^{-2}] and the stability ratio, respectively. R_i and R_j are the radii of the ith and jth particles. E_f is a lumping parameter that expresses the effect of the degree of agitation in the polymerization vessel on the primary particle coalescence rate.

The stability ratio W measures the effectiveness of the potential barrier in preventing the particles from coagulating.[40] This means that when there exists a repulsive energy barrier only a fraction $1/W$ of the collisions between particles lead to coalescence. The stability ratio was calculated according to the approximation proposed by Reerink and Overbeek.[41] The calculation of the total interaction energy V, which is given by the sum of the van der

Waals attractive, V_A, and electrostatic repulsive, V_R, potentials, follows the developments described in Kiparissides et al.,[35] Prindle and Ray,[42] Feeney et al.,[43] and Ottewil.[44]

For a given colloidal system, the attraction forces are assumed to be constant while the electrostatic repulsion forces can vary with the ionic strength of the medium. The reciprocal of the thickness of the electrical double layer, κ, appearing in the calculation of V_R, expresses the effect of the electrolyte concentration on the repulsion forces. The reciprocal Debye length, κ, is defined as[40,45]

$$\kappa = \left(\frac{e^2 N_A}{\varepsilon k T} \sum_i z_i^2 M_i \right)^{1/2} \tag{20}$$

where M_i is the concentration of the ions of type "i" and z_i is the corresponding valence number. Note that for a completely dissociated 1 : 1 electrolyte, eq. (20) can be expressed in terms of the concentration of the electrolyte (mol/L) and the absolute temperature of the solution. Assuming that the concentration of the ionic species of an unknown 1 : 1 electrolyte in VCM is equal to 1 μmol/L, the value of κ at 323 K will be approximately equal to[22] 1.3×10^7 m^{-1}.

Calculation of the Surface Potential

The surface potential can be calculated from the Poisson–Boltzmann equation assuming spherical symmetry and that the Debye–Hückel approximation for weakly charged particles is valid.[40,44] Integration of the charge that is contained from the surface of the particle to infinity provides (with a sign change) the total charge on the surface of the particle, Q_i. However, in dilute solutions, where the value of κ is very small, the surface of shear may be considered that coincides with the particle surface and, therefore, the particle potential can be approximated by the zeta potential of the charged particles:[40]

$$\psi_{0i} = \frac{Q_i}{4\pi\varepsilon R_i (1 + \kappa R_i)} \tag{21}$$

Equation (21) expresses the surface potential in terms of the particle charge, which is an unknown function of the particle size. Törnell et al.[22] proposed a semiempirical expression (22), which relates the primary particle radius to the total particle charge, to investigate the electrostatic stability of PVC primary particles:

$$Q_i = C_p R_i^p \tag{22}$$

p is an adjustable parameter taking values in the interval [0, 2]. Note that for $p = 0$, eq. (22) will satisfy the condition of constant electric charge for all particles. On the other hand, for $p = 2$ and $\kappa R_i \gg 1$, eq. (21) will satisfy the case of constant surface potential. The zeta potential of PVC primary particles has been measured by several investigators and found to be in the range of -80 to -120 mV. Cooper et al.[12] measured the electrophoretic mobility of PVC primary particles in liquid VCM and reported a value of -1.2×10^{-8} m^2 V^{-1} s^{-1} for PVC particles with a radius of 150 nm, which corresponds to a zeta potential of -80 mV (Rance[4]). Accordingly, the particle charge can be calculated from eq. (21) for $\kappa = 1.0 \times 10^7$ m^{-1} to be 1.57×10^{-17} Cb. The value of parameter C_p is then calculated from eq. (22) and the known values of Q_i and R_i for different values of the exponent p:

$$C_p = 1.57 \times 10^{-17} (1.5 \times 10^{-7})^{-p} \tag{23}$$

NUMERICAL SOLUTION OF THE POPULATION BALANCE

Prior to the numerical solution of eq. (5), the logarithmic transformation after Gelbard and Seinfield[46] was applied to eq. (5) to recast it into the following form:

$$\frac{\partial m(w,t)}{\partial t} + \frac{R_{pp}}{3[M_0]X \ln J} \frac{\partial [m(w,t)]}{\partial w} = \frac{J^{3w}}{2} \int_0^{Z'} \beta(x,z) m(x,t) m(z,t) \times (J^{3w} - J^{3z})^{-1} dz - m(w,t) \times \int_0^1 \beta(w,z) m(z,t)\, dz \tag{24}$$

$$w = \frac{\ln(D/D_{\min})}{\ln(D_{\max}/D_{\min})}; \quad z = \frac{\ln(D'/D_{\min})}{\ln(D_{\max}/D_{\min})} \tag{25}$$

$$x = \frac{\ln(J^{3w} - J^{3z})}{3 \ln J}; \quad J = \frac{D_{\max}}{D_{\min}}; \quad Z' = \frac{\ln(J^{3w} - 1)}{3 \ln J} \tag{26}$$

$$m(w,t) = n(D,t) \frac{dD}{dw} = n(D,t) D \ln J \tag{27}$$

$$m(x, t) = n(\Delta, t)\frac{d\Delta}{dx}$$
$$= D_{\min}(J^{3w} - J^{3z})^{1/3} n(\Delta, t) \ln J \quad (28)$$

$D_{\min}$ and $D_{\max}$ are the minimum and maximum diameter of primary particles, respectively.

Accordingly, the initial as well as the boundary conditions required for the integration of eq. (24) are written as

$$m(w, 0) = 0.0; \quad w \geq 0 \quad (29)$$

$$\frac{\partial m(0, t)}{\partial t} = -m(0, t)\int_0^1 \beta(0, z) m(z, t)\, dz + \frac{18 R_{\text{pm}} M_w}{\pi d_p (1 - \varphi_m) D_0^3} \ln J; \quad t > 0 \quad (30)$$

Several numerical methods have been proposed in the literature for solving partial integrodifferential equations.[47] These include finite-difference methods,[33,48,49] the method of moments,[50] the method of weighted residuals,[51] and collocation on finite elements.[52,53]

To simplify the numerical solution of eq. (24), the partial differential term $\partial m(w, t)/\partial w$ was assumed to be negligible. This is especially true in the early stages of polymerization when primary particles grow mainly by capturing unstable microdomains. Indeed, at low monomer conversions (< 5%), the rate of polymerization in the polymer-rich phase is approximately three orders of magnitude smaller than the corresponding rate in the monomer-rich phase.

Discretization of the Population Balance

To solve the integrodifferential population balance eq. (24), the whole range of variation of the dimensionless diameter w was divided into a suite of equally spaced diameters, $w_1, \ldots, w_N$ and eq. (24) was approximated by a system of N differential equations. w_N was set equal to one corresponding to the maximum size of the primary particles (i.e., $D_{\max}$ = 1000 nm).

The set of N differential equations obtained from the discretization of the population balance eq. (24) is written as follows:

$$\frac{d_{M_i}(w_i, t)}{dt} = \frac{J^{3w_i}}{2}\int_0^{z_i'} \beta(x_i, z) m_i(x_i, t) m_i(z, t) \times (J^{3w_i} - J^{3z})^{-1}\, dz - m_i(w_i, t) \times \int_0^1 \beta(w_i, z) m_i(z, t)\, dz \quad (31)$$

$$w_i = \frac{\ln(D_i/D_{\min})}{\ln J}; \quad J = \frac{D_{\max}}{D_{\min}} \quad (32)$$

$$x_i = \frac{\ln(J^{3w_i} - J^{3z})}{3 \ln J}; \quad Z_i' = \frac{\ln(J^{3w_i} - 1)}{3 \ln J} \quad (33)$$

The corresponding initial as well as the boundary conditions required for the integration of eq. (31) become:

$$m_i(w_i, 0) = 0.0; \quad w_i \geq 0; \quad i = 1, \ldots, N \quad (34)$$

$$\frac{d_{M_1}(w_1, t)}{dt} = -m_1(w_1, t)\int_0^1 \beta(w_1, z) m_1(z, t)\, dz + \frac{18 R_{\text{pm}} M_w}{\pi d_p (1 - \varphi_m) D_0^3} \ln J \quad (35)$$

The total number of primary particles per unit volume of the reaction medium will be given by the zero moment of the number-diameter density function:

$$N(t) = \int_{w_0}^{w_N} m(w, t)\, dw = \int_{D_0}^{D_N} n_D(D, t)\, d(D) \quad (36)$$

Accordingly, the mean primary particle diameter, D_{pq}, can be calculated by the general equation[54]

$$(D_{pq})^{p-q} = \frac{\int_{D_0}^{D_N} D^p n_D(D, t)\, dD}{\int_{D_0}^{D_N} D^q n_D(D, t)\, dD} \quad (37)$$

where the indices p and q ($p > q$) can take the values p = 1, 2, 3 and q = 0, 1, 2. For p = 1 and q = 0, eq. (37) defines the arithmetic mean particle diameter.

Solution of the Population Balance

The final system of ordinary differential eqs. (31) was solved iteratively using two different integration methods[54] (e.g., the Gear's predictor-corrector method and a variable step-size fourth-order Runge–Kutta method). Both integration methods required the initial value of the number of primary particles,

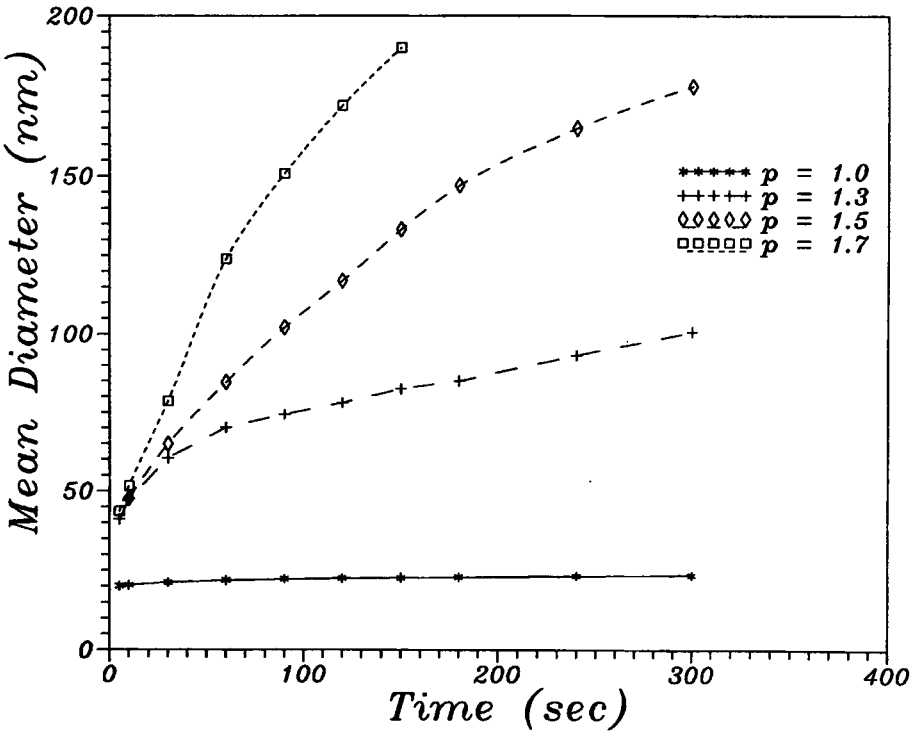

Figure 2 Effect of the total particle charge (parameter p) on the variation of the mean primary particle diameter with time ($\kappa = 1 \times 10^7$ m^{-1}; $T = 323$ K; initiator: LP, 1% w/w).

m_i, as well as a subroutine to calculate the gradient dm_i/dt at the discrete points $w_1, w_2, \ldots, w_N$. The various integral terms were calculated at each time step using a composite Simpson's rule. No significant differences were found between the results obtained by the two integration methods.

In all simulations, D_0 was set equal to 20 nm (diameter of the basic particles) and the value of D_N was set equal to 1000 nm. The number of collocation points, N, used to discretize the primary particle-size distribution into a set of ordinary differential equations, was set equal to 100. Although the use of a greater number of discretization points (e.g., 200) increased exponentially the computational effort, it did not improve significantly the simulation results.

The calculation of the integral terms required an iterative procedure. To integrate the system of N differential eqs. (31) from $t - \Delta t$ to t, the integral terms were initially approximated using the known discrete values of the number diameter density function, m_i, at time $t - \Delta t$ (iteration one). Accordingly, the system of N differential equations was numerically integrated and the new values of m_i were used to reevaluate the integral terms (iteration two). The iterative procedure was repeated several times (e.g., 3–4 iterations) until the satisfaction of the following convergence criterion:

$$\int_{V_0}^{V_N} V_{N_v}(V, t)\, dV = \int_{D_0}^{D_N} \frac{\pi D^3}{6} n_D(D, t)\, dD = \frac{[M_0]XM_w}{d_p(1 - \varphi_m)} \quad (38)$$

Equation (38) implies that the total volume of the primary particles, given by the first moment of the number-volume density function, must be equal to the volume of the monomer–swollen polymer phase calculated in terms of the overall monomer conversion. Notice that the monomer conversion is obtained from the integration of eq. (15).

RESULTS AND DISCUSSION

In the present section, simulation results obtained from the numerical solution of the population balance model (5) are presented showing the time evolution of the primary particle-size distribution in a batch PVC polymerization reactor. The effects of

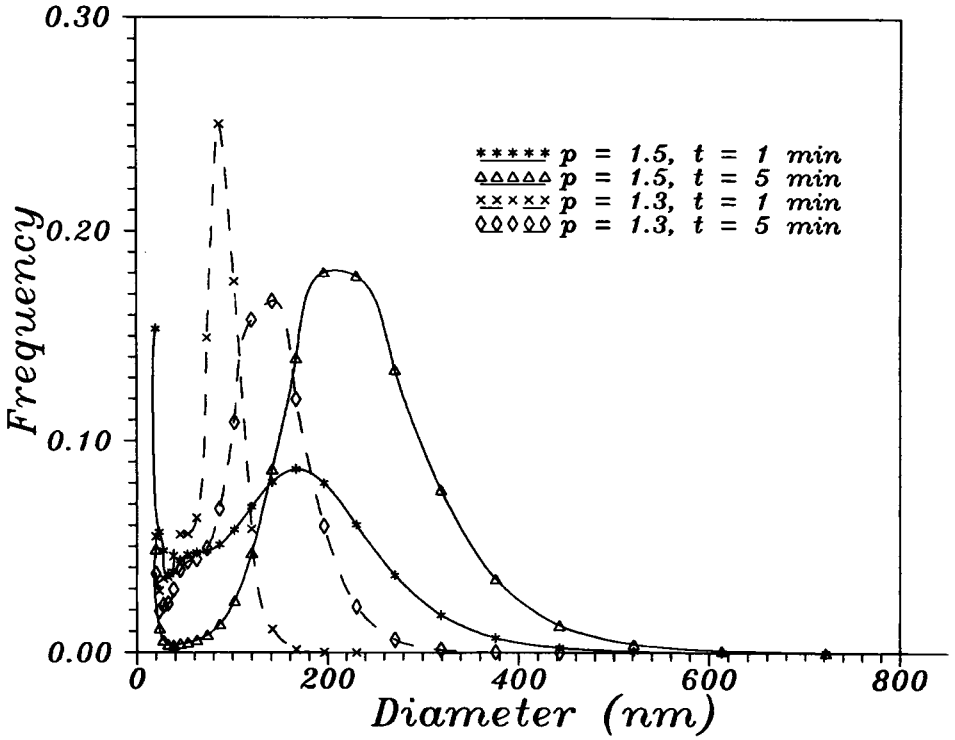

Figure 3 Time evolution of the primary particle-size distribution for two different values of the parameter p ($\kappa = 1 \times 10^7$ m^{-1}; $T = 323$ K; initiator: LP, 1% w/w).

the ionic strength of the medium, total particle charge, temperature, degree of agitation, initial concentration, and type of initiator on the average primary particle size and the total number of primary particles are quantitavely analyzed and compared with the experimental data of Willmouth et al.[19] and Törnell and Uustalu.[27]

As already discussed in the previous section, the total electric charge of a primary particle, Q_i, depends on the particle radius, R_i, and the parameter p [eq. (22)]. In this way, we can account for the variation of the surface potential, ψ_{0i}, with the size of the primary particles. In Figure 2, the mean primary particle diameter is plotted against the polymerization time for different values of the exponent p. In all simulated cases, the reciprocal Debye length was set equal to 1×10^7 m^{-1} and the temperature at 323 K. As can be seen for $p = 1.0$, the mean particle diameter is approximately constant and equal to the initial diameter of the microdomains (20 nm). On the other hand, as the value of p increases ($p > 1$), the growth rate of primary particles increases.

Figure 3 depicts the time evolution of primary particle-size distribution in a batch reactor for two different values of the parameter p. The results were obtained for $\kappa = 1 \times 10^7$ m^{-1} and a polymerization temperature of 323 K. Figure 3 shows a clear shift of the particle population toward higher diameters as the polymerization proceeds for both values of the parameter p. Note that at $t = 1$ min the primary particle-size distribution has two characteristic mode diameters corresponding to the basic and primary particle population, respectively. However, as the size of the primary particles increases, the coalescence rate constant between basic and primary particles increases, which results in the disappearance of the first characteristic mode diameter of the bimodal particle distribution. The corresponding values of the monomer conversion at 1 and 5 min of polymerization time are 0.1 and 0.7%. Higher aggregation rates are obtained as the value of the exponent p increases. For $p = 1.5$, the size of the primary particles exhibits a higher growth rate due to the higher rate of coalescence between unstable basic and primary particles.

The effect of the ionic strength (i.e., reciprocal Debye length, κ) on the time evolution of the total number and the mean primary particle diameter is shown in Figures 4 and 5. The results were obtained for $p = 1.2$ and a polymerization temperature of 323 K. It has been postulated[35] that an increase of the value of κ (i.e., increase of the ionic strength of the

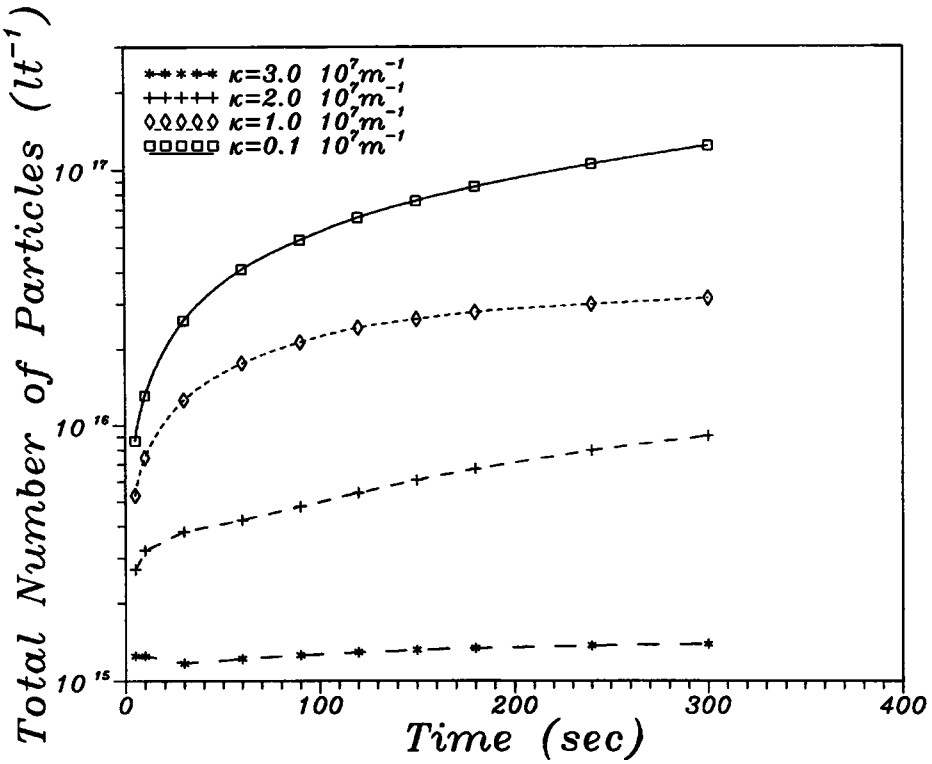

Figure 4 Effect of the reciprocal Debye length, κ, on the variation of the total number of primary particles with time (p = 1.2; T = 323 K; initiator: LP, 1% w/w).

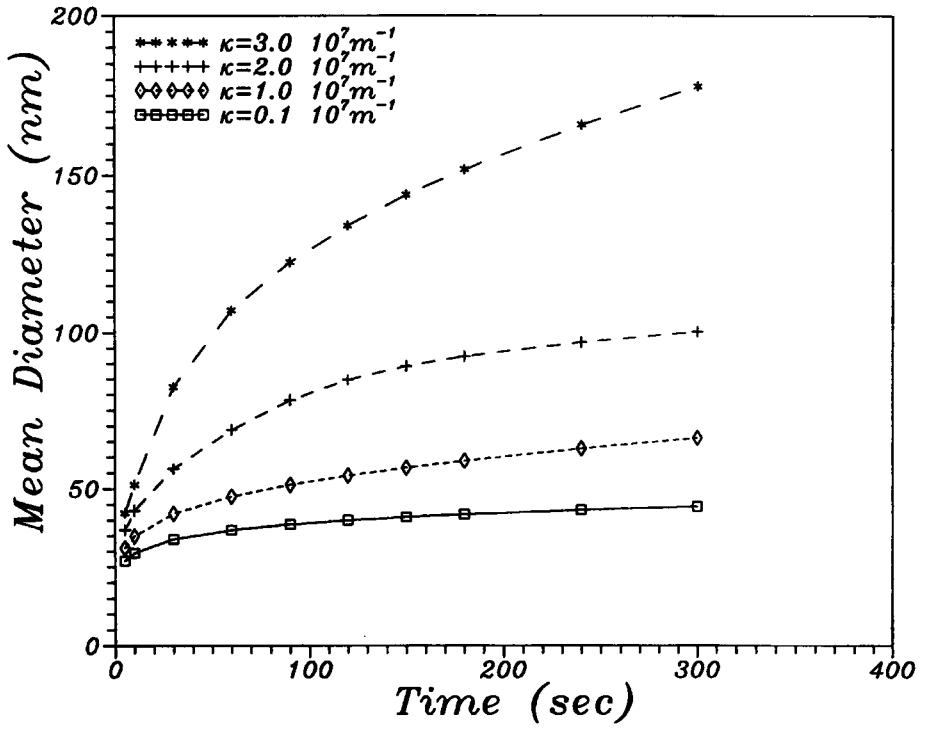

Figure 5 Effect of the reciprocal Debye length, κ, on the variation of the mean primary particle diameter with time (p = 1.2; T = 323 K; initiator: LP, 1% w/w).

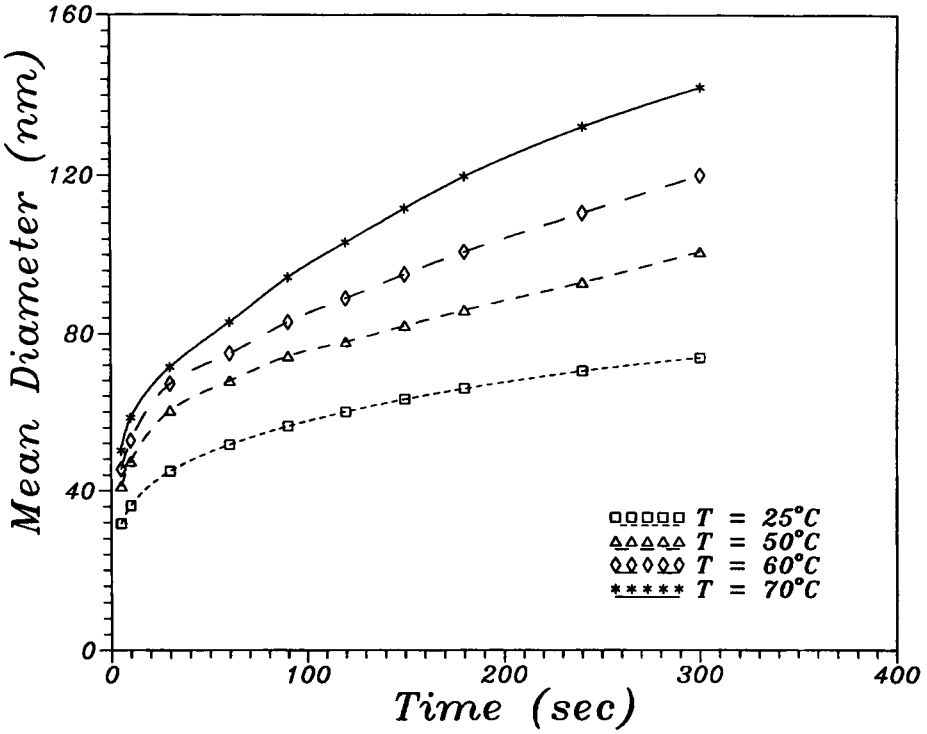

Figure 6 Effect of temperature on the variation of the mean particle diameter with time ($\kappa = 1 \times 10^7$ m^{-1}; $p = 1.3$; initiator: LP, 1% w/w).

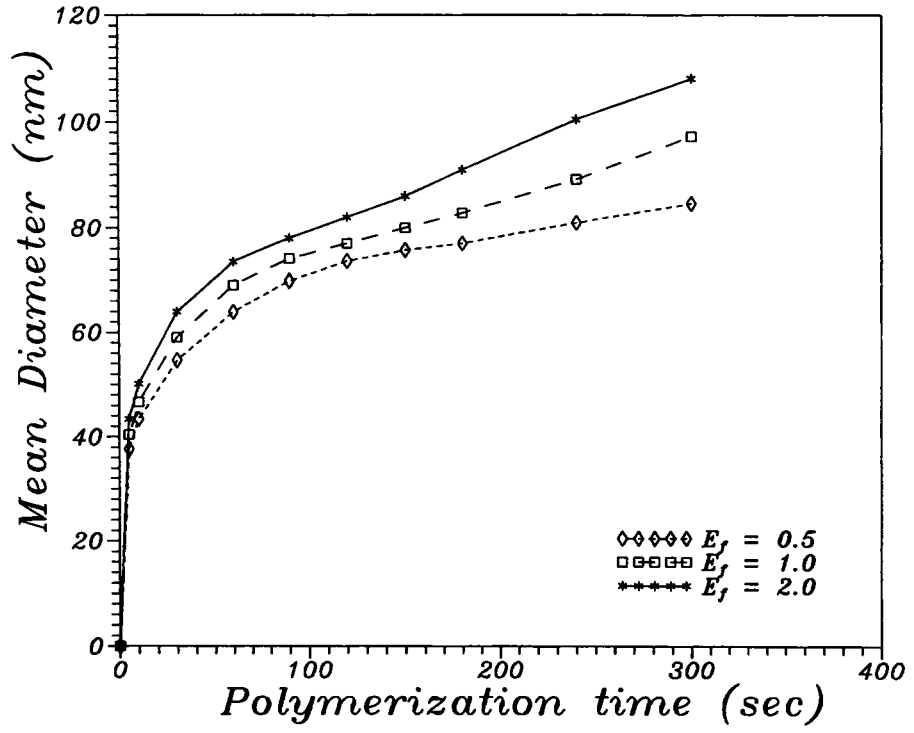

Figure 7 Effect of agitation on the variation of the mean particle diameter with time ($\kappa = 1 \times 10^7$ m^{-1}; $T = 323$ K; $p = 1.3$; initiator: LP, 1% w/w).

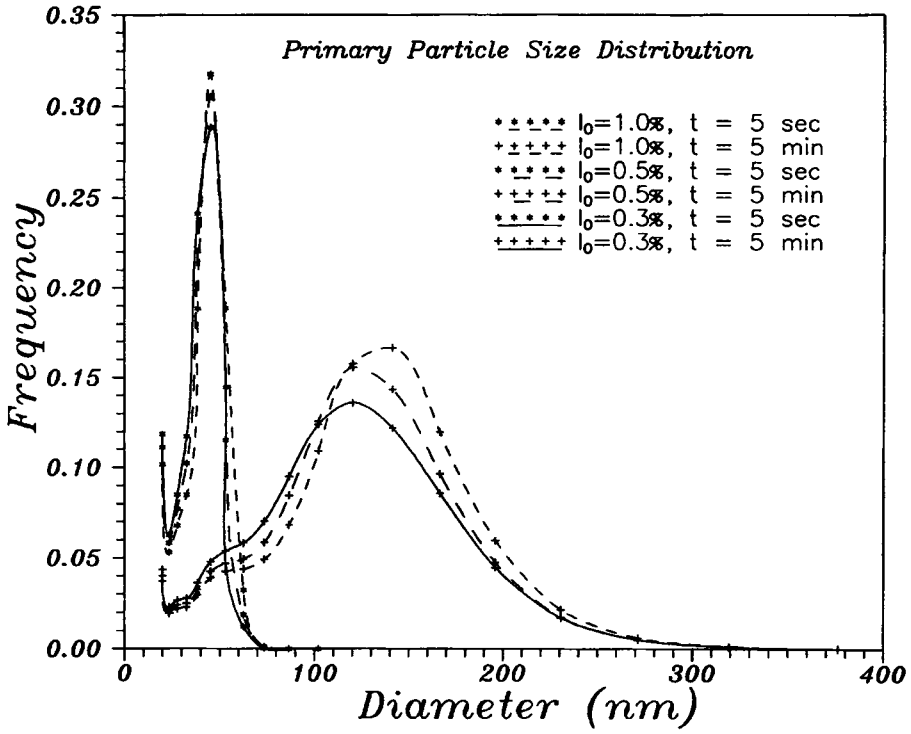

Figure 8 Time evolution of the primary particle size-distribution for different values of the initial initiator concentration ($\kappa = 1 \times 10^7$ m^{-1}; $T = 323$ K; $p = 1.3$; initiator: LP).

medium) results in a decrease of the particle surface potential, ψ_{0i}, which is accompanied by a decrease of the repulsion forces as well as of the stability of the primary particles. As a consequence, the primary particle size increases while the total number of primary particles decreases. Note that the value of κ varies from 0.1 to 4.0 $\times$ 10^7 m^{-1}.[22]

Figure 6 depicts the effect of the polymerization temperature on the time evolution of the mean primary particle diameter. It is known that the polymerization rate increases with temperature. Furthermore, as the temperature increases, the maximum energy barrier, V_{max}, decreases, resulting in an increase of the coalescence rate constant β_{ij}, and of the mean particle diameter.

The influence of the agitation rate on the primary particle coalescence rate was indirectly taken into consideration through the introduction of a lumped empirical parameter, E_f [see eq. (19)]. According to the results of Figure 7, as the rate of agitation decreases, E_f, the coalescence rate constant, β_{ij}, decreases. As a consequence, the growth of primary particles due to particle coalescence decreases while the total number of primary particles increases. However, it should be pointed out that the dependence of E_f on the rate of agitation can exhibit a complex U-shaped behavior, which means that E_f can either increase or decrease with rpm, depending on the range of variation of rpm.

The effect of the initial initiator concentration (i.e., dilauroyl peroxide) on the time evolution of the primary particle-size distribution is illustrated in Figure 8. It can be seen that at the very early stages of polymerization (e.g., reaction time of 5 s) the primary particle-size distribution is not influenced by the initial initiator concentration. However, at longer polymerization times, (e.g., t = 5 min), the number-diameter density function shifts to larger diameters and the mean diameter increases with increasing values of $[I]_0$.

In Figures 9 and 10, the model predictions are compared with the experimental data of Willmouth et al.[19] on the mean primary particle diameter and the total number of primary particles at two different temperatures. The numerical values of the parameters used in these simulations were D_{min} = 20 nm, D_{max} = 1000 nm, $E_f = 1.0$, $p = 1.5$, $\kappa = 1.3 \times 10^7$ m^{-1} at $T = 50$°C, $\kappa = 1.6\ 10^7$ m^{-1} at $T = 35$°C, $[I]_0 = 1\%$ w/v. It can be seen that model predictions for the mean particle diameter are in excellent agreement with the experimental data. On the other hand, the predicted number of primary particles is of the same order of magnitude with the experimentally measured values of N. In view of the large experimental

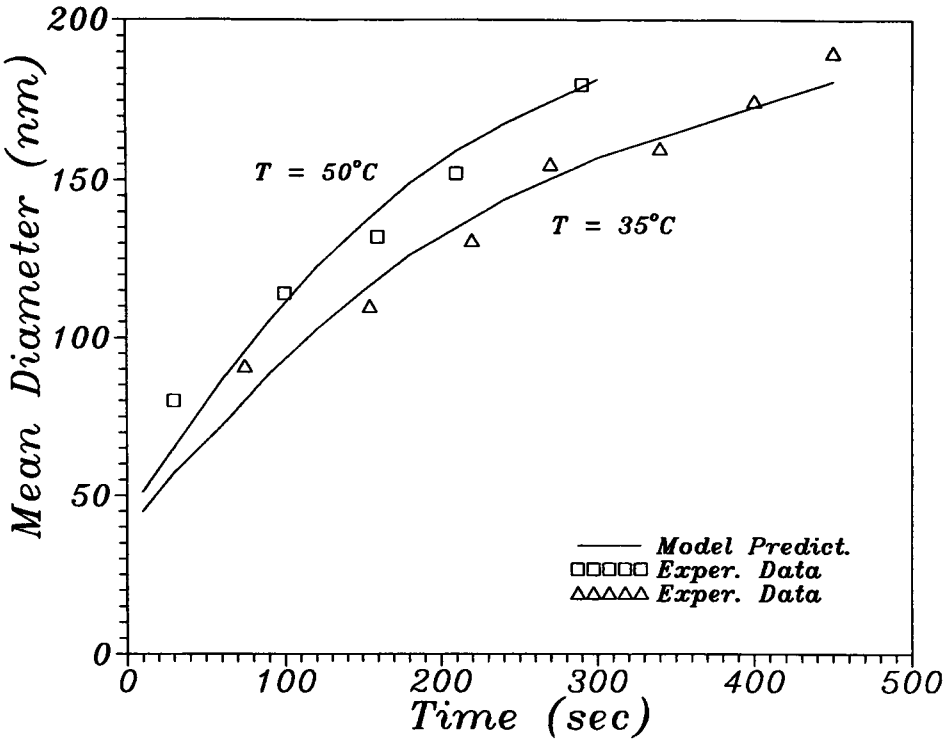

Figure 9 Experimental[19] and theoretical simulation results on the variation of the mean primary particle diameter with time ($\kappa = 1.3 \times 10^7$ m^{-1} at 50°C; $\kappa = 1.6 \times 10^7$ m^{-1} at 35°C; $p = 1.5$; $E_f = 1.0$; initiator: LP, 1% w/v).

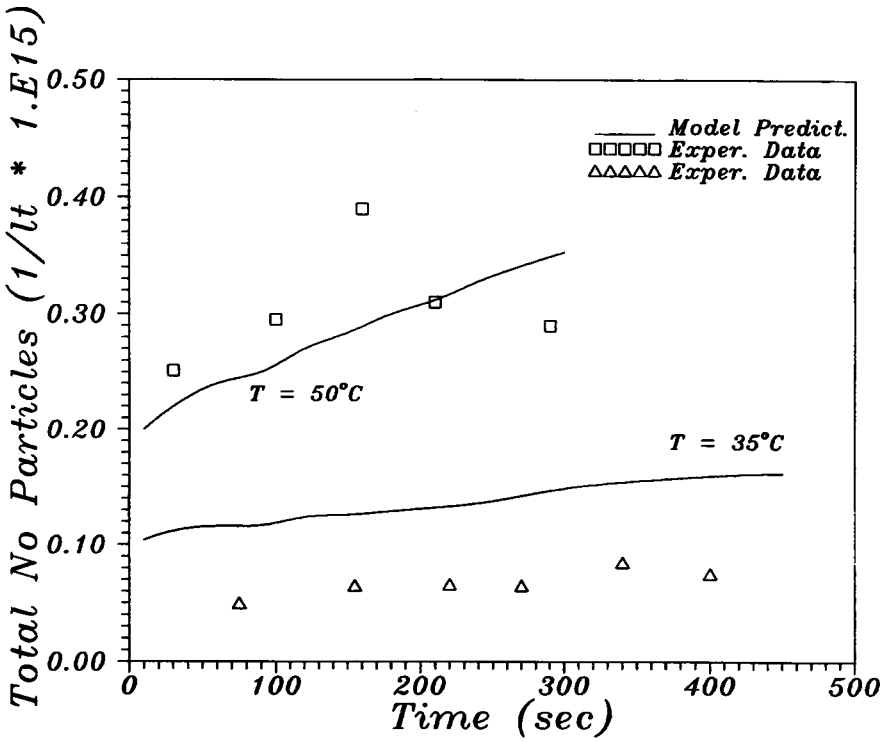

Figure 10 Experimental[19] and theoretical simulation results on the variation of the total number of primary particles with time ($\kappa = 1.3 \times 10^7$ m^{-1} at 50°C; $\kappa = 1.6 \times 10^7$ m^{-1} at 35°C; $p = 1.5$; $E_f = 1.0$; initiator: LP, 1% w/v).

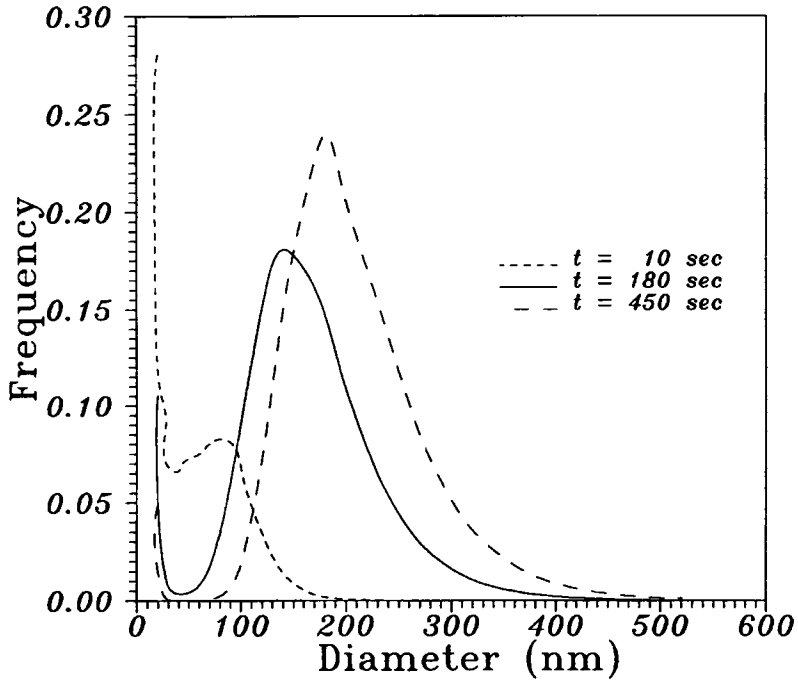

Figure 11 Time evolution of the primary particle-size distribution. Experimental conditions as in Figures 9 and 10.

errors in the measurement of the primary particles, the model predictions are in satisfactory agreement with experimental data (Fig. 10).

The corresponding model predictions on the evolution of the primary particle-size distribution at three different polymerization times: t = 10, 180,

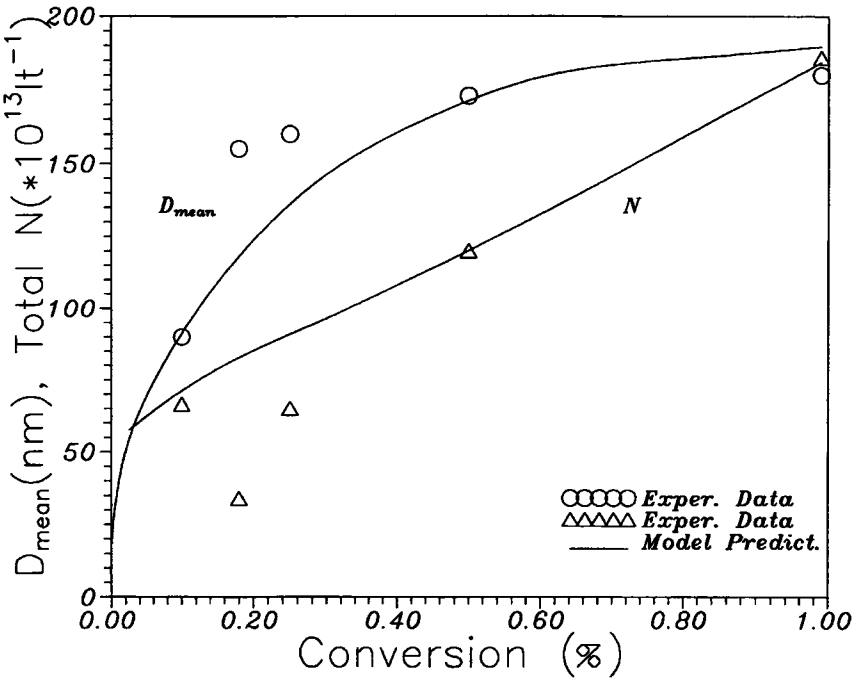

Figure 12 Experimental[27] and theoretical simulation results on the variation of the mean particle diameter and total number of primary particles with time ($\kappa = 1.4 \times 10^7$ m^{-1}; T = 59°C; p = 1.42; E_f = 1.8; initiator: LP, 0.092% w/w).

and 450 s and constant temperature $T = 35°C$, are shown in Figure 11. According to the results of this figure, it can be postulated that at the initial stages of polymerization a bimodal particle distribution is obtained. As the polymerization proceeds (i.e., at 180 and 450 s), the first characteristic mode diameter decreases, the distribution becomes narrower, while the mean particle size shifts to larger values.

Finally, in Figure 12, a comparison between the model predictions and the experimental data of Törnell and Uustalu[27] for the mean diameter and the total number of primary particles is shown. The parameters used for the theoretical simulations were $\kappa = 1.4 \times 10^7\ m^{-1}$, $T = 59°C$, $p = 1.42$, $E_f = 1.8$, and $[I]_0 = 0.092\%$ w/w. It is interesting to note that the present theoretical model is capable of predicting the time evolution of both the mean particle diameter and total number of primary particles equally well. Note that the experimental data were collected from a 1 L bulk VCM polymerization reactor agitated at a constant speed of 1.5 m/s.

CONCLUSIONS

In the present article, a mathematical model has been developed that quantitatively describes the time evolution of the primary particle-size distribution during the batch polymerization of VCM. The effect of the most important process parameters on the mean diameter as well as on the total number of the PVC primary particles has been thoroughly investigated. It can be postulated that an increase of the primary particle mean diameter is favored by an increase of the ionic strength of the medium, the total particle charge (parameter p), the initial initiator concentration, the temperature, and the agitation.

The above process parameters, except the polymerization temperature, have exactly the opposite effect on the total number of primary particles, i.e., the total number of primary particles increases as the mean particle diameter decreases. Finally, the predictive capabilities of the developed theoretical model have been successfully demonstrated by comparison of model predictions with the experimental data of Willmouth et al.[19] and Törnell and Uustalu[27] for the bulk polymerization of VCM.

NOMENCLATURE

I_v	rate of particle growth ($m^3\ s^{-1}$)
κ	reciprocal Debye length (m^{-1})
M_i	concentration of "i" type ions (geq m^{-3})
$n_v(V, t)\ dV$	number of primary particles in the size range V and $V + dV$ (# m^{-3})
N_A	Avogandro's number
t	time (s)
T	temperature (K)
V	volume of primary particle (m^3)
W	stability ratio, dimensionless
X	fractional monomer conversion

Greek Letters

β_{ij}	coalescence rate constant between particles "i" and "j" ($m^2\ s^{-1}$)
ψ_0	particle surface potential (V)

REFERENCES

1. J. B. Cameron, A. J. Lundeen, J. M. McCulley, and P. A. Schwab, *J. Appl. Polym. Sci. Appl. Polym. Symp.*, **36,** 133 (1981).
2. G. Butters, *Particulate Nature of PVC,* Applied Science, London, 1982.
3. R. H. Burgess, *Manufacturing and Processing of PVC,* Applied Science, London, 1982.
4. D. G. Rance, in *Polymer Colloids,* R. Buscall, T. Corner, and J. F. Stageman, Eds., Elsevier, Amsterdam, 1985, p. 289.
5. M. Langsam, in *Encyclopedia of PVC,* 2nd ed., L. I. Nass and C. A. Heiberger, Eds., Marcel Dekker, New York, Basel, 1986, Vol. 1, p. 48.
6. B. E. Törnell, *Polym. Plast. Technol. Eng.*, **27,** 1 (1988).
7. T. Y. Xie, A. E. Hamielec, P. E. Wood, and D. R. Woods, *Polymer,* **32**(3), 537 (1991).
8. T. Y. Xie, A. E. Hamielec, P. E. Wood, and D. R. Woods, *J. Vinyl Technol.*, **13**(1), 2 (1991).
9. H. G. Yuan, G. Kalfas, and W. H. Ray, *J. Macrom. Sci.-Rev. Macromol. Chem. Phys.*, **C31**(2, 3), 215 (1991).
10. E. L. Zichy, *J. Macromol. Sci., Chem.*, **A11,** 1205 (1977).
11. J. C. Wilson and E. L. Zichy, *Polymer,* **20,** 264 (1979).
12. W. D. Cooper, R. M. Speirs, J. C. Wilson, and E. L. Zichy, *Polymer,* **20,** 265 (1979).
13. D. G. Rance and E. L. Zichy, *Polymer,* **20,** 267 (1979).
14. J. A. Davidson and D. E. Witenhafer, *J. Polym. Sci. Polym. Phys. Ed.*, **18,** 51 (1980).
15. D. G. Rance and E. L. Zichy, *Pure Appl. Chem.*, **53,** 377 (1981).
16. J. Ugelstad, P. C. Moerk, F. K. Hansen, K. H. Kaggerund, and T. Ellingsen, *Pure Appl. Chem.*, **53,** 323 (1981).
17. M. W. Allsopp, *Pure Appl. Chem.*, **53,** 449 (1981).
18. H. Nilsson, C. Silvegren, and B. Tornell, *Angew. Makromol. Chem.*, **112,** 125 (1983).

19. F. M. Willmouth, D. G. Rance, and K. M. Henman, *Polymer,* **25,** 1185 (1984).
20. B. E. Törnell and J. M. Uustalu, *J. Vinyl Techn.,* **4,** 53 (1982).
21. B. E. Törnell and J. M. Uustalu, *Polymer,* **27,** 250 (1986).
22. B. E. Törnell, J. M. Uustalu, and B. Jönsson, *Colloid Polym. Sci.,* **264,** 4439 (1986).
23. J. M. Uustalu, *J. Polym. Sci. Part A Polym. Chem.,* **24,** 1609 (1986).
24. H. Nilsson, C. Silvegren, and J. Uustalu, *Polym. Commun.,* **24,** 268 (1983).
25. P. V. Smallwood, *Polymer,* **27,** 1609 (1986).
26. A. Guyot, *Makromol. Chem. Macromol. Symp.,* **10/11,** 461 (1987).
27. B. E. Törnell and J. M. Uustalu, *J. Appl. Polym. Sci.,* **35,** 63 (1988).
28. G. Weickert, R.-D. Klodt, B. Platzer, K.-D. Weissenborn, and I. Henschel, *Angew. Makromol. Chem.,* **164,** 59 (1988).
29. G. Weickert, B. Platzer, K.-D. Weissenborn, R.-D. Klodt, and I. Henschel, *Angew. Makromol. Chem.,* **164,** 79 (1988).
30. I. Henschel, B. Platzer, and G. Weickert, *Angew. Makromol. Chem.,* **172,** 47 (1989).
31. I. Henschel and B. Platzer, *Angew. Makromol. Chem.,* **172,** 59 (1989).
32. P. V. Smallwood, *Makromol. Chem. Macromol. Symp.,* **29,** 1 (1989).
33. W. H. Ray, S. K. Jain, and R. Salovey, *J. Appl. Polym. Sci.,* **19,** 1297 (1975).
34. C. Kiparissides, *Makromol. Chem. Macromol. Symp.,* **35/36,** 171 (1990).
35. C. Kiparissides, I. Moustakis, and A. E. Hamielec, *J. Appl. Polym. Sci.,* **49,** 445 (1993).
36. E. Sidiropoulou and C. Kiparissides, *J. Macrom. Sci. Chem.,* **A27**(3), 257 (1990).
37. A. H. Abdel-Alim and A. E. Hamielec, *J. Appl. Polym. Sci.,* **16,** 783 (1972).
38. H. Müller, *Kolloid-Reih,* **26,** 257 (1928).
39. N. Fuchs, *Z. Phys.,* **89,** 736 (1934).
40. R. J. Hunter, *Foundation of Colloid Science,* Clarendon Press, Oxford, 1987.
41. H. Reerink and J. Th. G. Overbeek, *Disc. Faraday Soc.,* **18,** 74 (1954).
42. J. C. Prindle and W. H. Ray, Paper presented at the Annual AIChE Meeting, New York, Nov. 1987.
43. P. J. Feeney, D. H. Napper, and R. G. Gilbert, *Macromolecules,* **20,** 2922 (1987).
44. R. H. Ottewill, in *An Introduction to Polymer Colloids,* F. Candau and R. H. Ottewill, Eds., Kluwer, Dordrecht, The Netherlands, 1990, pp. 129–157.
45. D. H. Napper, *Polymeric Stabilization of Colloidal Dispersion,* Academic Press, London, 1983.
46. F. Gelbard and J. H. Seinfeld, *J. Comput. Phys.,* **28,** 357 (1978).
47. D. Ramkrishna, *Rev. Chem. Eng.,* **3,** 49 (1985).
48. E. Diamadopoulos, I. Zoubourtikoudis, and C. Kiparissides, *Colloid Polym. Sci.,* **268,** 306 (1990).
49. C. Kiparissides and S. R. Ponnuswamy, *Chem. Eng. Commun.,* **10,** 283 (1981).
50. G. Storti, M. Morbidelli, and S. Carra, in *Computer Applications in Applied Polymer Science II,* T. Provder, Ed., ACS Symposium Series 404, American Chemical Society, Washington, DC, 1989, Chap. 30.
51. P. Canu and W. H. Ray, *Comput. Chem. Eng.,* **15**(8), 549 (1991).
52. G. F. Carey and B. A. Finlayson, *Chem. Eng. Sci.,* **30,** 587 (1975).
53. R. Galvan and M. Tirrell, *Comput. Chem. Eng.,* **10**(1), 77 (1986).
54. E. G. Chatzi and C. Kiparissides, *Chem. Eng. Sci.,* **47**(2), 445 (1992).

Received February 25, 1994
Accepted March 24, 1994